Multiple Coulomb and Nuclear Excitation of ^{238}U with Very Heavy Ions*

Volker Oberacker and Gerhard Soff

A. W. Wright Nuclear Structure Laboratory, Yale University, New Haven, USA

and

Institut für Theoretische Physik der Johann Wolfgang Goethe Universität, Frankfurt am Main, Germany

(Z. Naturforsch. **32a**, 1465–1476 [1977]; received October 22, 1977)

Coupled channel calculations for Coulomb and nuclear excitation of the systems ^{136}Xe-^{238}U and ^{238}U-^{238}U have been performed using the rotation-vibration model. The impact parameter-, energy- and spin-dependence of the excitation probabilities are discussed for the ground state-, β- and γ-band up to $J^{\pi} = 36^{+}$. It is shown that the energy levels and quadrupole matrix elements are strongly influenced by the rotation-vibration interaction. Analytic expressions for the elastic and coupling potentials are presented.

1. Introduction

In connection with first experiments at GSI concerning positron creation and Coulomb fission in collisions of very heavy ions, an accurate theoretical description of Coulomb and nuclear excitation of ^{238}U becomes necessary: The spontaneous and induced positron production in overcritical fields[1] is accompanied by internal pair creation following nuclear Coulomb excitation[2–6,32]. An experimental separation of both processes should be feasible by their different spectra. Furthermore, measurements of the K-vacancy probability as well as the spectroscopy of superheavy electronic quasimolecules are only possible if nuclear background contributions like conversion processes can be subtracted. Recently fission of ^{238}U induced by ^{136}Xe projectiles below the interaction barrier has been observed[7–9]. At low incident energy, the experimental data are interpreted as Coulomb fission events[8] even though a small influence of transfer reactions cannot be ruled out. These data can be explained quantitatively[10,33] by considering the rotation-vibration interaction (RVI) which lowers the Coulomb fission cross section by at least one order of magnitude compared with the theoretical results of Ref. [11], neglecting RVI. It is needless to mention that Coulomb excitation is a powerful tool for the examination of collective nuclear properties[12–15], especially in the actinide region[16–21]. All these facts demonstrate the importance of extensive Coulomb excitation calculations for very heavy nuclei. The calculations reported here are the first ones including not only the ground state rotational band but also several higher bands up to spin $36\hbar$. For this purpose the standard COULEX-program by Winther and de Boer[22] was modified to include about 80 levels, allowing for 9 magnetic substates per level. Additionally, strong interaction effects were taken into account in the excitation and in the relative motion of the nuclei.

After a short review of the general excitation formalism in Sect. 2 we derive analytic expressions for the coupling potentials, especially the nuclear part, which are valid also in the overlap region ($r < R_{01} + R_{02}$). In Sect. 4 a description of the intrinsic Hamiltonian is given and the calculated energy spectrum is compared with experimental data. We evaluate the collective quadrupole matrix elements entering the excitation code and tabulate numerical values for several interband matrix elements which are related to the γ-transition rates. Finally, we present typical numerical results concerning angular distributions, spin distributions and excitation functions for the system ^{136}Xe-^{238}U and ^{238}U-^{238}U. The strong influence of the rotation-vibration interaction on the excitation of high spin states is extensively discussed.

* Work supported by the Bundesministerium für Forschung und Technologie (BMFT), and by the Gesellschaft für Schwerionenforschung (GSI).

Reprint requests to Dr. V. Oberacker, Institut für Theoretische Physik der J. W. Goethe-Universität, Robert-Mayer-Straße 10, *D-6000 Frankfurt/M. I.*

2. Coupled Channel Equations for Coulomb and Nuclear Excitation

We consider inelastic heavy ion scattering with projectile energies in the vicinity of the Coulomb barrier. If the nuclear surfaces are separated by a distance $d \gtrsim 4$ fm, the interaction is of pure electromagnetic nature. In heavy ion collisions, where the nuclei do not overlap, the maximum relative velocity amounts to $v/c \lesssim 0.1$. Therefore retardation effects as well as the magnetic interaction, being proportional to $(v/c)^2 \approx 0.01$, can be neglected. Hence the excitation is mainly determined by the electric multipole-multipole interaction.

For projectile energies in the region of the Coulomb barrier the strong interaction also becomes important. The attractive nuclear forces lead to interference effects in angular distributions and excitation functions[12–14, 23].

The total Hamiltonian in the c.m. system has the following structure

$$H(1,2,\boldsymbol{r}) = H_0(1) + H_0(2) + W(1,2,\boldsymbol{r}) + T_{\mathrm{rel}} \tag{2.1}$$

where $H_0(n)$, $n=1,2$ describes the unperturbed projectile and target nucleus, respectively. The potential W, containing the electromagnetic and strong interaction, depends on the intrinsic coordinates of both nuclei and the relative coordinate $\boldsymbol{r}$. T_{rel} is the kinetic energy of relative motion. The interaction W may be written in the form

$$W(1,2,\boldsymbol{r}) = U(\boldsymbol{r}) + V(1,2,\boldsymbol{r}), \tag{2.2}$$

where $U(\boldsymbol{r})$ denotes the monopole-monopole part and V the coupling potential for projectile and target excitation. Because of the large Sommerfeld-parameter $\eta = Z_1 Z_2 e^2/\hbar v \gg 1$ in collisions of heavy nuclei the excitation mechanism may be treated in semiclassical approximation. The classical trajectory $\boldsymbol{r}(t)$ is obtained by solving Hamilton's equations with the elastic potential $U(\boldsymbol{r})$. Figure 1 shows the classical trajectory in a ^{238}U-^{238}U collision at $E_{\mathrm{lab}} = 1785$ MeV. Compared with the Rutherford hyperbola the distance of closest approach changes from $R_{\min} = 14.1$ fm to 13.0 fm for an impact parameter $b = 2.485$ fm.

Since we have separated the relative motion, the time dependent Schrödinger equations reads

$$[H_0(1) + H_0(2) + V(1,2,\boldsymbol{r}(t))]\,\psi(1,2,t) = i\hbar \frac{\partial}{\partial t}\psi(1,2,t) \tag{2.3}$$

The dominant part of the coupling potential is given by the monopole-multipole interaction (see Section 3).

$$V(1,2,\boldsymbol{r}) \approx V(1,\boldsymbol{r}) + V(2,\boldsymbol{r}). \tag{2.4}$$

The first term in Eq. (2.4) only contains the intrinsic coordinates of the projectile and therefore causes projectile excitation, while the second term concerns the target nucleus. Using Eq. (2.4) the Schrödinger equation (2.3) separates ($i=1,2$)

$$[H_0(\xi_i) + V(\xi_i, \boldsymbol{r}(t))]\,\psi(\xi_i,t) = i\hbar \frac{\partial}{\partial t}\psi(\xi_i,t). \tag{2.5}$$

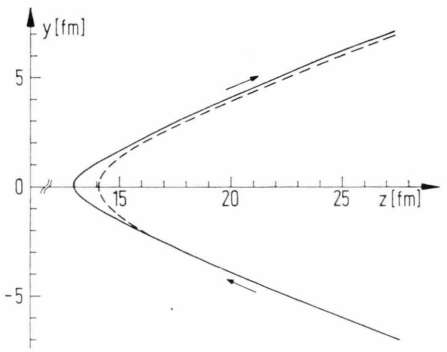

Fig. 1. Classical trajectory in the elastic potential $U(r)$ for a ^{238}U-^{238}U collision at impact parameter $b = 2.485$ fm (solid line). The incident energy $E_{\mathrm{lab}} = 1785$ MeV exceeds the Coulomb barrier by about 25%. The corresponding Rutherford hyperbola is given by the dashed line.

We expand the total wave function ψ in terms of the eigenstates $\varphi_m(\xi_i)$ of the unperturbed Hamiltonian $H_0(\xi_i)$

$$\psi(\xi_i,t) = \sum_m a_m(t)\,\varphi_m(\xi_i)\exp[-(i/\hbar)\,E_m t], \tag{2.6}$$

which leads to the following set of linear coupled differential equations for the occupation amplitudes.

$$\dot{a}_n(t) = (i\hbar)^{-1}\sum_m a_m(t)\,\langle\varphi_n(\xi)\,|\,V(\xi,\boldsymbol{r}(t))\,|\,\varphi_m(\xi)\rangle \times \exp\{(i/\hbar)(E_n - E_m)\,t\}. \tag{2.7}$$

The asymptotic excitation probabilities

$$P_n^{\mathrm{cb}}(t\to+\infty) = |a_n(t\to+\infty)|^2 \tag{2.8}$$

are calculated numerically with a coupled channel code including also the strong interaction.

3. Elastic and Coupling Potentials

In general the nucleus-nucleus potential consists of a Coulomb and nuclear part. If the nuclear

surfaces do not overlap the Coulomb interaction is given by the usual multipole expansion[24]

$$V_{\mathrm{Coul}}(\boldsymbol{r}) = \frac{Z_1 Z_2 e^2}{r} + \sum_{\substack{l_1, l_2 \geq 1 \\ m_1, m_2}} B_{l_1 l_2}^{m_1 m_2} (-1)^{l_1} r^{-l_1 - l_2 - 1} \times M_1^*(E l_1, m_1) M_2^*(E l_2, m_2) Y_{l_1+l_2, -m_1-m_2}(\Omega) \tag{3.1}$$

with

$$B_{l_1 l_2}^{m_1 m_2} = \frac{(-1)^{m_1+m_2} (4\pi)^{3/2}}{[(2l_1+1)(2l_2+1)(2l_1+2l_2+1)]^{1/2}} \times \left[\frac{(l_1+l_2+m_1+m_2)!\,(l_1+l_2-m_1-m_2)!}{(l_1+m_1)!\,(l_1-m_1)!\,(l_2+m_2)!\,(l_2-m_2)!} \right]^{1/2} \tag{3.2}$$

and the electric multipole operator

$$M(E l, m) = \int \varrho_p(\boldsymbol{r})\, r^l\, Y_{lm}^*(\Omega)\, \mathrm{d}\tau\,. \tag{3.3}$$

We note that the relative coordinate $\boldsymbol{r}$ is directed form nucleus 2 to nucleus 1. The nuclear potential can be evaluated within the framework of the extended liquid drop model[25, 26]. It is a functional of the nuclear density distribution $\varrho(\boldsymbol{r}_i)$ of both ions and contains the Yukawa, compression and symmetry energy

$$V_{\mathrm{nucl}}(\boldsymbol{r}) = V_{\mathrm{Yuk}}(\boldsymbol{r}) + V_{\mathrm{comp}}(\boldsymbol{r}) + V_{\mathrm{sym}}(\boldsymbol{r})\,. \tag{3.4}$$

In sudden approximation, $\varrho = \varrho(\boldsymbol{r}_1) + \varrho(\boldsymbol{r}_2)$, these potentials are related to the basic Yukawa integral

$$Y(\boldsymbol{r}, \mu, \varrho_1, \varrho_2) = \frac{1}{4\pi} \iint \varrho(\boldsymbol{r}_1) \frac{\exp[-|\boldsymbol{r}_1 - \boldsymbol{r}_2 + \boldsymbol{r}|/\mu]}{|\boldsymbol{r}_1 - \boldsymbol{r}_2 + \boldsymbol{r}|} \varrho(\boldsymbol{r}_2)\, \mathrm{d}\tau_1\, \mathrm{d}\tau_2 \tag{3.5}$$

in the following manner

$$\begin{aligned} V_{\mathrm{Yuk}}(\boldsymbol{r}) &= V_0 \left[Y(\boldsymbol{r}, \mu, \varrho_1, \varrho_2) - \mu^2 \lim_{\nu \to 0} \frac{1}{\nu^2} Y(\boldsymbol{r}, \nu, \varrho_1, \varrho_2) \right], \\ V_{\mathrm{comp}}(\boldsymbol{r}) &= \frac{C}{\varrho_0} \lim_{\nu \to 0} \frac{1}{\nu^2} \left[Y(\boldsymbol{r}, \nu, \varrho_1, \varrho_2) - \tfrac{1}{2} Y(\boldsymbol{r}, \nu, \varrho_0, \varrho_0) \right], \\ V_{\mathrm{sym}}(\boldsymbol{r}) &= \frac{G}{\varrho_0} \left(1 - 2\frac{Z_1}{A_1}\right)\left(1 - 2\frac{Z_2}{A_2}\right) \lim_{\nu \to 0} \frac{1}{\nu^2} Y(\boldsymbol{r}, \nu, \varrho_1, \varrho_2)\,. \end{aligned} \tag{3.6}$$

For the equilibrium density in infinite nuclear matter we take the value $\varrho_0 = 0.17\ \mathrm{fm}^{-3}$ obtained by Bethe[27]. The compression and symmetry constants are fixed by certain stability conditions[11] to be $C = 30$ MeV and $G = 70$ MeV, respectively. In the calculations the range μ of the Yukawa force enters as free parameter; it was varied between 1.0 and 1.2 fm. The corresponding strength V_0 depends on μ and can be deduced e.g. from the height of the Coulomb barrier.

In analogy to the Coulomb interaction, Eq. (3.1), the Yukawa integral in Eq. (3.5) can be expanded in multipoles. As suggested in Ref. [25] for spherical nuclei, we first Fourier-transform the integrand in Eq. (3.5)

$$\frac{\exp[-|\boldsymbol{r}_1 - \boldsymbol{r}_2 + \boldsymbol{r}|/\mu]}{|\boldsymbol{r}_1 - \boldsymbol{r}_2 + \boldsymbol{r}|} = \frac{1}{2\pi^2} \int \mathrm{d}^3k\, \frac{\exp[i\,\boldsymbol{k}(\boldsymbol{r}_1 - \boldsymbol{r}_2 + \boldsymbol{r})]}{k^2 + 1/\mu^2} \tag{3.7}$$

and expand the plane waves $e^{i\boldsymbol{k}\boldsymbol{u}}$ into partial waves with angular momentum L

$$\exp[i\,\boldsymbol{k}\,\boldsymbol{u}] = 4\pi \sum_{L,M} i^L j_L(k\,u)\, Y_{LM}(\Omega_k)\, Y_{LM}^*(\Omega_u)\,. \tag{3.8}$$

Inserting the expressions (3.7) and (3.8) into the Yukawa integral Y one obtains

$$Y(\boldsymbol{r}, \mu, \varrho_1, \varrho_2) = \sum_{l,m} f_{lm}(r, \mu, \varrho_1, \varrho_2)\, Y_{lm}^*(\Omega) \tag{3.9}$$

with

$$\begin{aligned} f_{lm}(r, \mu, \varrho_1, \varrho_2) = 8(4\pi)^{-1/2} \sum_{l_1 m_1 l_2 m_2} i^{l_1 - l_2 + l} [(2l_1+1)(2l_2+1) \\ \times (2l+1)]^{1/2} \begin{pmatrix} l_1 & l_2 & l \\ 0 & 0 & 0 \end{pmatrix} \begin{pmatrix} l_1 & l_2 & l \\ m_1 & m_2 & m \end{pmatrix} \int_0^\infty \mathrm{d}k\, \frac{k^2}{k^2 + 1/\mu^2} j_l(k\,r)\, A_{l_1 m_1}(k_1, \varrho_1)\, A_{l_2 m_2}(k, \varrho_2). \end{aligned} \tag{3.10}$$

The formfactors A_{lm} are defined by

$$A_{lm}(k, \varrho) = \int \mathrm{d}\tau\, \varrho(\boldsymbol{r})\, j_l(k\, r)\, Y^*_{lm}(\Omega)\,. \quad (3.11)$$

In the following we restrict ourselves to the monopole-multipole part of the interaction in Eqs. (3.1) and (3.10) which is known to be dominant from Coulomb excitation experiments.

The formulas simplify considerably

$$V_{\mathrm{Coul}}(\boldsymbol{r}) = \frac{Z_1 Z_2\, e^2}{r} + \sum_{l \geqq 1, m} \frac{4\pi}{2l+1}\, r^{-l-1} \quad (3.12)$$
$$\times [(-1)^l Z_2\, e\, M_1(E\,l, m) + Z_1\, e\, M_2(E\,l, m)]\, Y_{lm}(\Omega)$$

and similarly Eq. (3.10) becomes

$$f_{lm}(r, \mu, \varrho_1, \varrho_2) = \frac{8(4\pi)^{-1/2}}{1+\delta_{l0}} \int_0^\infty \frac{k^2\, \mathrm{d}k}{k^2 + 1/\mu^2}\, j_l(k\, r)$$
$$\times [A_{00}(k, \varrho_1)\, (-1)^m\, A_{l-m}(k, \varrho_2)$$
$$+ (-1)^l\, A_{00}(k, \varrho_2)$$
$$\times (-1)^m\, A_{l-m}(k, \varrho_1)]\,. \quad (3.13)$$

Since the Coulomb forces in a heavy-ion collision mainly excite the collective degrees of freedom such as rotations, surface vibrations, and giant resonances, we describe the nucleus in terms of the collective surface variables α_{lm}

$$R(\Omega) = R_0[1 + \sum_{l,m} \alpha_{lm}\, Y^*_{lm}(\Omega)]\,. \quad (3.14)$$

Assuming homogeneous density distributions ϱ_1 and ϱ_2 we obtain for the electric multipole operator

$$M(E\,l, m) = \frac{3Z\, e\, {R_0}^l}{4\pi}\, \alpha^*_{lm} + O(\alpha^2_{lm}) \quad (3.15)$$

and similarly the formfactor is given by

$$A_{lm}(k, \varrho) = (4\pi)^{1/2}\, \varrho\, \frac{{R_0}^2}{k}\, j_1(k\, R_0)\, \delta_{l0}\, \delta_{m0}$$
$$+ \varrho\, {R_0}^3\, j_l(k\, R_0)\, \alpha^*_{lm} + O(\alpha^2_{lm})\,, \quad (3.16)$$

where we have restricted ourselves to terms linear in the surface variables α_{lm}. Combining Eqs. (3.16), (3.13), and (3.9) the Yukawa integral reads[28]

$$Y(\boldsymbol{r}, \mu, \varrho_1, \varrho_2) = 4\varrho_1\, \varrho_2\, R^2_{01}\, R^2_{02}[F(\mu, r, R_{01}, R_{02})$$
$$+ R_{01} \sum_{l \geqq 1, m} (-1)^l\, \alpha^{(1)}_{lm}\, Y^*_{lm}(\Omega)\, G_l(\mu, r, R_{01}, R_{02})$$
$$+ R_{02} \sum_{l \geqq 1, m} \alpha^{(2)}_{lm}\, Y^*_{lm}(\Omega)\, G_l(\mu, r, R_{02}, R_{01})]\,. \quad (3.17)$$

In Eq. (3.17) the following abbreviations have been used

$$F(\mu, x, y, z) = \int_{-\infty}^{+\infty} \frac{\mathrm{d}k}{k^2 + 1/\mu^2}\, j_0(k\, x)\, j_1(k\, y)\, j_1(k\, z)$$
$$G_l(\mu, x, y, z) = \int_{-\infty}^{+\infty} \frac{k\, \mathrm{d}k}{k^2 + 1/\mu^2}\, j_l(k\, x)\, j_l(k\, y)\, j_1(k\, z)\,. \quad (3.18)$$

The integration over the momentum space in Eq. (3.18) can be done by means of the theory of residues[23].

We have calculated also the Coulomb potential for two overlapping nuclei which is contained in our formalism, namely

$$V_{\mathrm{Coul}}(\boldsymbol{r}) = \frac{4\pi Z_1 Z_2\, e^2}{A_1 A_2} \lim_{\nu \to \infty} Y(\boldsymbol{r}, \nu, \varrho_1, \varrho_2)\,. \quad (3.19)$$

For the evaluation of the various nuclear potentials in Eq. (3.6) and the Coulomb potential one needs the quantities F and G_l as well as their limites $\mu \to 0$ and $\mu \to \infty$. For $l=2$ the corresponding analytic expressions are given in appendix A.

For well separated nuclei ($r > R_{01} + R_{02}$) only the first term of the Yukawa potential contributes to the nuclear potential. Hence, it results

$$V_{\mathrm{nucl}}(\boldsymbol{r}) = U_{\mathrm{Yuk}}(r) + \sum_{m=-2}^{+2} [T^{(1)}_{2\,\mathrm{Yuk}}(r)\, \alpha^{(1)}_{2m}$$
$$+ T^{(2)}_{2\,\mathrm{Yuk}}(r)\, \alpha^{(2)}_{2m}]\, Y^*_{2m}(\Omega)\,, \quad (3.20)$$

$$U_{\mathrm{Yuk}}(r) = g\, \frac{e^{-r/\mu}}{r} \quad (3.21)$$

with

$$g = 4\pi\, V_0\, \mu^2\, \varrho_1\, \varrho_2\, R^2_{01}\, R^2_{02}$$
$$\times \left[\left(\frac{\mu}{R_{01}}\right)^2 \sinh\frac{R_{01}}{\mu} - \frac{\mu}{R_{01}} \cosh\frac{R_{01}}{\mu}\right]$$
$$\times \left[\left(\frac{\mu}{R_{02}}\right)^2 \sinh\frac{R_{02}}{\mu} - \frac{\mu}{R_{02}} \cosh\frac{R_{02}}{\mu}\right]$$

and

$$T^{(2)}_{2\,\mathrm{Yuk}}(r) = h\, f_2(r) \quad (3.22)$$

with

$$h = 8\pi\, V_0\, \varrho_1\, \varrho_2\, R^2_{01}\, R^3_{02}[f_2(R_{02}) + f_2(-R_{02})]$$
$$\times [-f_1(R_{01}) + f_1(-R_{01})]\,, \quad (3.22)$$

$$f_1(x) = \tfrac{1}{2} \exp(-x/\mu) \left[\frac{\mu}{x} + \left(\frac{\mu}{x}\right)^2\right], \quad \text{continued}$$

$$f_2(x) = \tfrac{1}{2} \exp(-x/\mu) \left[\frac{\mu}{x} + 3\left(\frac{\mu}{x}\right)^2 + 3\left(\frac{\mu}{x}\right)^3\right].$$

The corresponding coupling potential for projectile excitation, $T^{(1)}_{2\,\mathrm{Yuk}}(r)$, is obtained from Eq. (3.22) by interchanging the nuclear radii R_{01} and R_{02}.

In Figure 2 the elastic potential $U(r)$ and the radial part of the coupling potential $T_2(r)$ are plotted for the system ^{238}U-^{238}U. The dashed curves correspond to Coulomb interaction only. In contrast to lighter systems like ^{12}C-^{12}C no quasimolecular minimum[29] is found in the elastic potential due to the predominance of the repulsive Coulomb force. Obviously the strong interaction lowers the Coulomb barrier by about 50 MeV (c.m.s.).

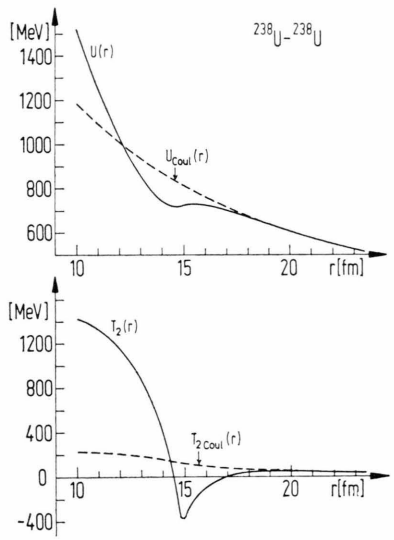

Fig. 2. Elastic potential $U(r)$ and radial part of the quadrupole coupling potential $T_2(r)$ for ^{238}U-^{238}U. The range and strength of the Yukawa potential amount to $\mu = 1.2$ fm and $V_0 = -300$ MeV fm, respectively. The dashed curves are calculated with Coulomb interaction only.

Concerning the coupling potential it is seen that the nuclear forces diminish the Coulomb excitation [caused by $T_{2\,\mathrm{Coul}}(r)$], when the nuclei reach a distance less than about 20.0 fm during the scattering process. $T_2(r)$ has a maximum at $r_m = 19.2$ fm with $T_2(r_m) = 46.33$ MeV. It is important to realize that total Coulomb-nuclear interference,

$$T_2(R_{\mathrm{cr}} = 17.0\,\mathrm{fm}) = 0\,,$$

takes place even before the nuclei touch at $R_{01} + R_{02} = 14.9$ fm.

4. Collective Hamiltonian and Quadrupole Matrix Elements

Since we are mainly interested in Coulomb and nuclear excitation of deformed even-even nuclei, we use the Hamiltonian of the rotation-vibration model (RVM)[30, 31]

$$H_0 = H_{\mathrm{rot}} + H_{\mathrm{vib}} + H_{\mathrm{rot-vib}} \tag{4.1}$$

to describe the nucleus.

Neglecting the rotation-vibration interaction $H_{\mathrm{rot-vib}}$ one obtains the following energy spectrum

$$E^{\mathrm{I}}_{Kn_2n_0} = \frac{\varepsilon}{2}\,[I(I+1) - K^2] + (\tfrac{1}{2}K + 1 + 2n_2)\,E_\gamma + (n_0 + \tfrac{1}{2})\,E_\beta \tag{4.2}$$

and the corresponding eigenfunctions

$$\Phi^{\mathrm{IM}}_{Kn_2n_0}(\vartheta_j, \xi, \eta) = \left(\frac{2I+1}{16\pi^2(1+\delta_{K,0})}\right)^{1/2} \times [D^{\mathrm{I}*}_{\mathrm{MK}}(\vartheta_j) + (-1)^{\mathrm{I}}\,D^{\mathrm{I}*}_{M-K}(\vartheta_j)] \times U_{K,n_2}(\eta)\,v_{n_0}(\xi)\,. \tag{4.3}$$

The collective energy levels of the Hamiltonian H_0 are obtained by numerical diagonalization of $H_{\mathrm{rot-vib}}$ within the basis states given in Equation (4.3). For ^{238}U the six lowest rotational bands

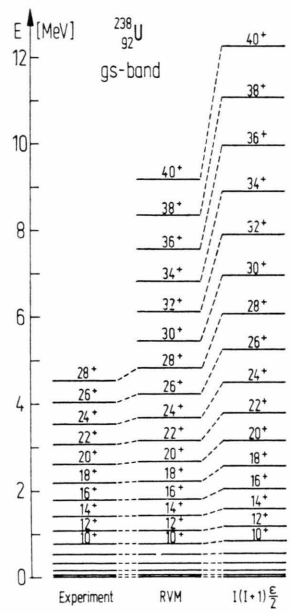

Fig. 3. Comparison between experimental[17, 21] and theoretical energy spectrum of the ground state rotational band. a) rotation-vibration model (RVM), b) symmetric rotor.

$|Kn_2n_0\rangle$ up to spin 40^+ were included. The energy parameters entering Eq. (4.2) were taken from the low energy spectrum of ^{238}U (Ref. [16]) and amount to $\varepsilon = 0.0137$, $E_\beta = 0.9948$ and $E_\gamma = 1.0445$ MeV. Figure 3 gives a comparison between experimental and theoretical energy levels of the ground state rotational band. The rotation-vibration interaction (RVI), which is equivalent to a centrifugal stretching of the nucleus, appreciably lowers the spectrum of the high spin states. We find $\Delta E = 0.5$, 1.5 and 3.0 MeV for $I = 20$, 30, and 40, respectively. Including RVI, the experimental ground state band [17, 21] is reproduced rather well. The theoretical predictions for the β- and γ-band as well as for the two phonon bands $|002\rangle$, $|201\rangle$ and $|400\rangle$ are presented in Figure 4. For the evaluation of the various excitation amplitudes in Eq. (2.7) we need the matrix elements $\langle\varphi_{n'}|V|\varphi_n\rangle$ of the coupling potential. Using the expression (3.12) and (3.17) these can be reduced to the matrix elements of the operators $M(El, m)$ and α_{lm}, which are in fact proportional to each other in lowest order α_{lm} (see Eq. (3.15)). The eigenstates φ_n are expanded in the basis (4.3)

$$\varphi_n^{\mathrm{IM}} = \sum_{Kn_2n_0} C^{\mathrm{I}*}_{n,Kn_2n_0} \Phi^{\mathrm{IM}}_{Kn_2n_0}, \tag{4.4}$$

where the expansion coefficients C follow from the diagonalization procedure. Using the Wigner-Eckart theorem

$$\langle\varphi_{n'}^{\mathrm{I'M'}}|M(El,m)|\varphi_n^{\mathrm{IM}}\rangle = (-1)^{\mathrm{I'-M'}} \times \begin{pmatrix} I' & l & I \\ -M' & m & M \end{pmatrix} \langle\varphi_{n'}^{\mathrm{I'}}\|M(El)\|\varphi_n^{\mathrm{I}}\rangle \tag{4.5}$$

it is sufficient to evaluate the reduced matrix elements of the electric multipole operator. Inserting the expansion (4.4) we obtain

$$\langle\varphi_{n'}^{\mathrm{I'}}\|M(E2)\|\varphi_n^{\mathrm{I}}\rangle = \sum_{\substack{Kn_2n_0 \\ K'n_2'n_0'}} C^{\mathrm{I'}}_{n',K'n_2'n_0'} C^{\mathrm{I}*}_{n,Kn_2n_0} \times \langle\Phi^{\mathrm{I'}}_{K'n_2'n_0}\|M(E2)\|\Phi^{\mathrm{I}}_{Kn_2n_0}\rangle. \tag{4.6}$$

According to Ref. [31] the collective quadrupole operator in second order α_{lm} can be expressed by the intrinsic coordinates ξ, η and the Euler angles ϑ_j

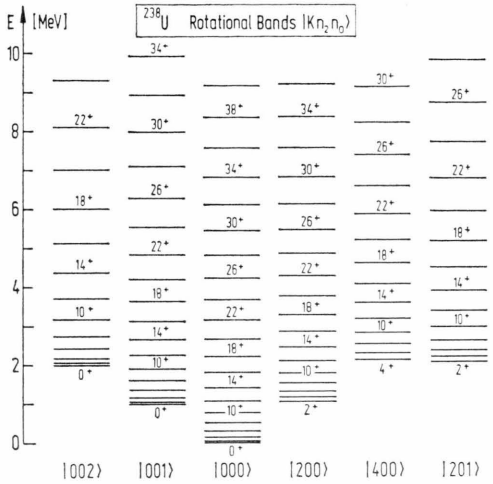

Fig. 4. Rotational bands built on top of several β- and γ-vibrational levels in ^{238}U, as predicted by the RVM.

$$\langle\Phi^{\mathrm{I'}}_{K'n_2'n_0'}\|M(E2)\|\Phi^{\mathrm{I}}_{Kn_2n_0}\rangle = \frac{3ZeR_0^2}{4\pi}\Big\{\langle I'K'\|D^2_{00}\|IK\rangle \times\Big[\beta_0(1+\alpha)\,\delta_{K'K}\,\delta_{n_2'n_2}\,\delta_{n_0'n_0} + (1+2\alpha)\,\delta_{K'K}\,\delta_{n_2'n_2}\langle n_0'|\xi|n_0\rangle + \frac{\alpha}{\beta_0}\,\delta_{K'K}\,\delta_{n_2'n_2}\langle n_0'|\xi^2|n_0\rangle - 2\frac{\alpha}{\beta_0}\langle K'n_2'|\eta^2|Kn_2\rangle\,\delta_{n_0'n_0}\Big] + \langle I'K'\|D^2_{0\,-2} + D^2_{0\,+2}\|IK\rangle\Big[\langle K'n_2'|\eta|Kn_2\rangle\,\delta_{n_0'n_0}(1-2\alpha) - \langle K'n_2'|\eta|Kn_2\rangle\langle n_0'|\xi|n_0\rangle\frac{2\alpha}{\beta_0}\Big]\Big\}. \tag{4.7}$$

β_0 describes the equilibrium deformation and $\alpha = \frac{2}{7}(5/\pi)^{1/2}\beta_0$. The numerical value of β_0 can be calculated from the transition matrix element $\langle 2^+g\|M(E2)\|0^+g\rangle$ leading to $\beta_0 = 0.264$ for ^{238}U. The matrix elements of the rotation matrices are easily evaluated to be

$$\langle I'K'\|D^2_{00}\|IK\rangle = (2I'+1)^{1/2}(I'\,2\,I|K'OK), \quad \langle I'K'\|D^2_{0\,-2} + D^2_{0\,+2}\|IK\rangle = \left(\frac{2I'+1}{(1+\delta_{KO})(1+\delta_{K'O})}\right)^{1/2} \times[(I'\,2\,I|K'\,2K) + (-1)^{\mathrm{I}}(I'\,2\,I|-K'\,2K) + (I'\,2\,I|K'-2K)]. \tag{4.8}$$

For the ξ-vibrational matrix elements one obtains

$$\langle n_0' \,|\, \xi \,|\, n_0 \rangle = \beta_0\, y[(n_0+1)^{1/2}\,\delta_{n_0',n_0+1} + (n_0)^{1/2}\,\delta_{n_0',n_0-1}]\,,$$
$$\langle n_0' \,|\, \xi^2 \,|\, n_0 \rangle = \beta_0^2\, y^2[(n_0+2)^{1/2}(n_0+1)^{1/2}\,\delta_{n_0',n_0+2} + (2n_0+1)\,\delta_{n_0'n_0} + (n_0-1)^{1/2}\,n_0{}^{1/2}\,\delta_{n_0',n_0-2}] \quad (4.9)$$

with the abbreviation $y=(3\,\varepsilon/(2E_\beta))^{1/2}$. The η-vibrational matrix elements follow from the general expression (13) in Ref. [30]

$$\langle K'\,n_2' \,|\, \eta \,|\, K\,n_2 \rangle = \beta_0 \frac{x}{\sqrt{2}}\,\delta_{K',K-2}[(\tfrac{1}{2}K+n_2)^{1/2}\,\delta_{n_2'n_2} - (n_2+1)^{1/2}\,\delta_{n_2',n_2+1}]$$
$$+ \beta_0 \frac{x}{\sqrt{2}}\,\delta_{K',K+2}\,[(\tfrac{1}{2}K+n_2+1)^{1/2}\,\delta_{n_2'n_2} - (n_2)^{1/2}\,\delta_{n_2',n_2-1}]$$
$$\langle K'\,n_2' \,|\, \eta^2 \,|\, K\,n_2 \rangle = \beta_0{}^2 \frac{x^2}{2}\,\delta_{K'K}[-\,n_2{}^{1/2}(\tfrac{1}{2}K+n_2)^{1/2}\,\delta_{n_2',n_2-1}$$
$$+ (\tfrac{1}{2}K+1+2n_2)\,\delta_{n_2'n_2} - (n_2+1)^{1/2}(\tfrac{1}{2}K+n_2+1)^{1/2}\,\delta_{n_2',n_2+1}]\,, \quad (4.10)$$

where the coefficient x is given by $x=(3\,\varepsilon/E_\gamma)^{1/2}$.

Numerical results for the $E2$ transition matrix elements between the ground state band, which can be measured in Coulomb excitation experiments are listed in Table 1. They are generally enlarged by the rotation-vibration interaction. For the $10^+ \to 8^+$, $20^+ \to 18^+$ and $30^+ \to 28^+$ transition the change amounts to 5, 15 and 22%. On the other hand the interband matrix elements

$$(I+2)^+\,\beta \to I^+\,g \quad \text{and} \quad (I+2)^+\,\gamma \to I^+\,g$$

decrease and therefore we expect an enhancement of the Coulomb excitation probabilities for the ground state band.

Table 1. E2-transition matrix elements in the ground state band of ^{238}U calculated with and without rotation-vibration interaction (RVI).

Transition	$\langle I+2 \,\|\| M(\mathrm{E2}) \,\|\| I \rangle$ [$e\cdot b$]	
	with RVI	without RVI
2^+-0^+	3.51	3.51
4^+-2^+	5.67	5.62
6^+-4^+	7.24	7.09
8^+-6^+	8.60	8.30
10^+-8^+	9.85	9.34
12^+-10^+	11.0	10.3
14^+-12^+	12.2	11.1
16^+-14^+	13.3	12.0
18^+-16^+	14.4	12.7
20^+-18^+	15.4	13.4
22^+-20^+	16.4	14.1
24^+-22^+	17.4	14.7
26^+-24^+	18.3	15.3
28^+-26^+	19.2	15.9
30^+-28^+	20.1	16.5
32^+-30^+	20.9	17.0
34^+-32^+	21.6	17.6
36^+-34^+	22.3	18.1

5. Numerical Results

We solved the coupled channel Eqs. (2.7) numerically for ^{136}Xe-^{238}U and ^{238}U-^{238}U.

All levels of the gs-, β- and γ-band of the target nucleus below the spin dependent fission barrier E_f were taken into account (see Figure 4). By discretizing the continuum states above E_f according to [10], Coulomb fission could be studied simultaneously. In contrast to backward scattering where only magnetic substances $M=0$ are populated, it is necessary for the computation of angular distributions to include various magnetic substates for each level. Test runs showed a convergence of the results with $|M| \leq 4$ even at forward angles, which leads to a system of 630 coupled differential equations for the occupation amplitudes.

Figure 5 shows the Coulomb excitation probabilities P^{Cb} in a ^{238}U-^{238}U collision for some members of the ground state-, β- and γ-band as function of the c.m. scattering angle. The results are valid for target as well as projectile excitation. The bombarding energy E_{lab} corresponds to a distance of closest approach $r_{\min}=22.3$ fm between the nuclei which is far outside the range of nuclear forces. As a common feature one realizes that the excitation maximum is transferred from the low spin to the high spin states with increasing scattering angle. Some oscillation structures in the angular distribution are caused by virtual excitations of levels belonging not to the same rotational band. Concerning the gs-band, the Coulomb excitation probability reaches a maximum at $J^\pi=24^+$ for backward scattering with $P^{\mathrm{Cb}}(24^+)=8\cdot 10^{-2}$. For the 30^+ state we have $P^{\mathrm{Cb}}(30^+)=3\cdot 10^{-3}$, and for

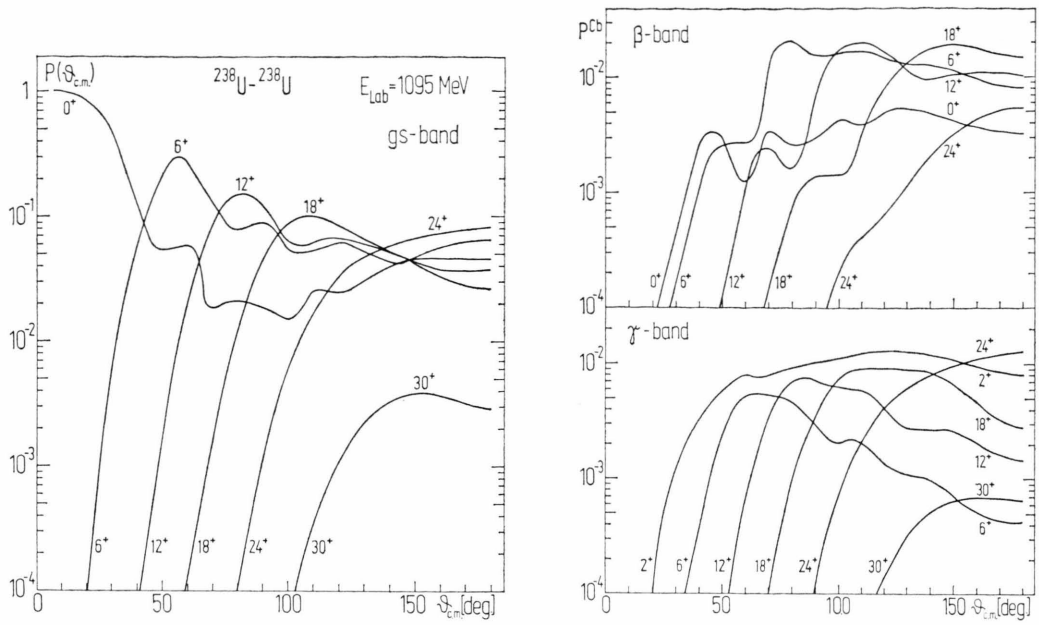

Fig. 5. Angular distribution (c.m.s.) of the Coulomb excitation probability in a ^{238}U-^{238}U collision for different members of the ground state- and the first β- and γ-vibrational band. The oscillatory structure, especially in the β-band, is explained in the text.

still higher spins the occupation probabilities fall off exponentially, so that the 36^+ level just below the fission barrier can hardly be observed in the experimental photon spectrum ($P^{Cb}(36^+) = 1 \cdot 10^{-5}$). The rotational bands built on the β- and γ-vibrational states are excited much less, for instance $P^{Cb}(30^+\gamma) = 6 \cdot 10^{-4}$ and $P^{Cb}(30^+\beta) = 3 \cdot 10^{-5}$.

The spin dependence of Coulomb excitation at fixed bombarding energy and scattering angle becomes even more transparent from Figure 6. A kind of "sawtooth" structure is observed being typical for rotational nuclei[18]. In the following we consider the ^{136}Xe-^{238}U collision at backward angles

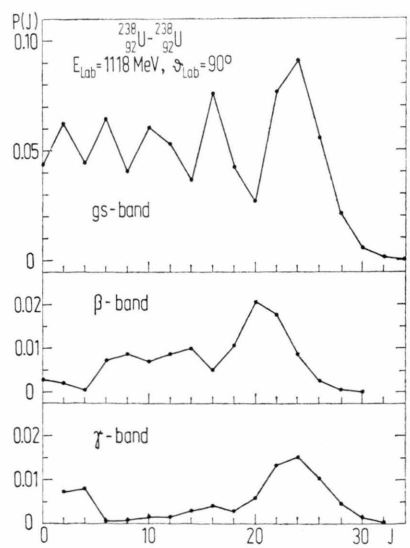

Fig. 6. Spin dependence of the Coulomb excitation probabilities at fixed bombarding energy and scattering angle. The "sawtooth"-structure is typical for rotational nuclei.

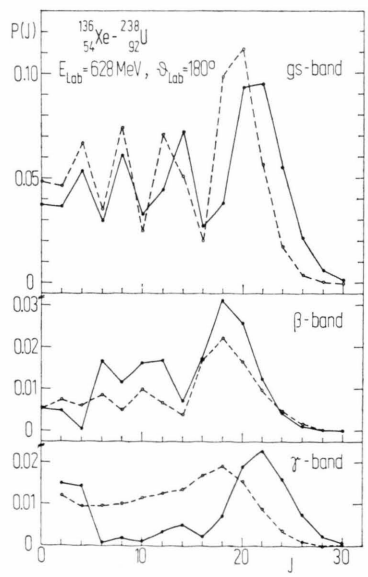

Fig. 7. As Fig. 6, but for the Xe-U system. The solid curves have been calculated with, the dashed curves without rotation-vibration interaction.

with $E_{lab} = 628$ MeV (Fig. 7), where the strong interaction can be neglected. P^{Cb} is plotted versus the angular momentum J. The calculation was done with and without rotation-vibration interaction (solid and dashed curves, respectively). As expected from the smaller energy difference between successive levels (see Fig. 3), and the enhancement of the $E2$-transition matrix elements the high spin states in the gs-band will be populated stronger. For the rotational members 22^+, 24^+ and 26^+ P^{Cb} differs by a factor of about 1.5, 3.0 and 5.5 with increasing tendency towards higher spins. On the other hand, the occupation of the β-vibrational states, which are most responsible for Coulomb fission, is reduced for $J^\pi \geqq 22^+$. From the excitation probabilities of the levels above the fission threshold we conclude that the theoretical Coulomb fission cross sections given in Ref. [11] for Xe-U will be reduced by at least

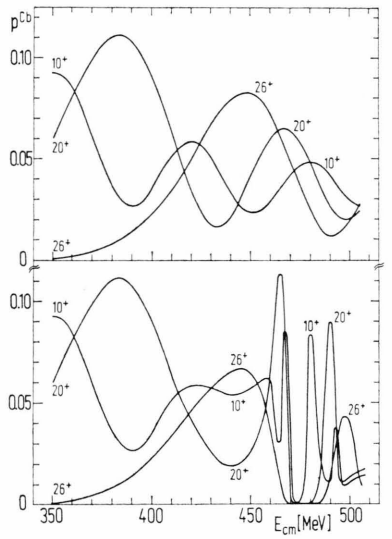

Fig. 8. Excitation functions for high spin states of the gs-band in ^{238}U, calculated for backward scattered ^{136}Xe projectiles. Upper part: pure Coulomb interaction; lower part: both Coulomb and nuclear excitation. Note the strong interference minimum around 470 MeV.

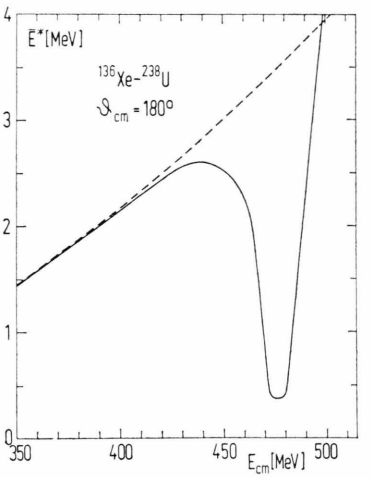

Fig. 10. Mean excitation energy of the ^{238}U target nucleus in a head-on collision of Xe-U as function of bombarding energy. The dashed curve corresponds to pure Coulomb excitation.

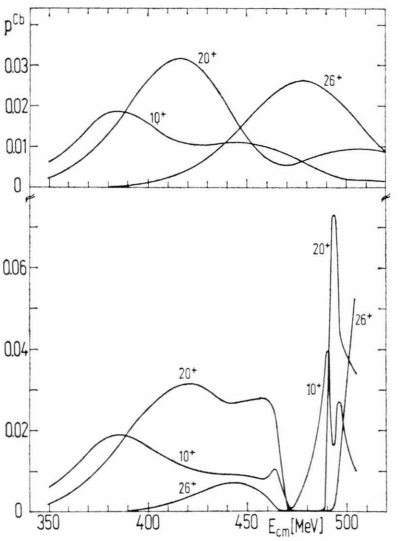

Fig. 9. As Fig. 8, but for first β-vibrational band in ^{238}U.

one order of magnitude at low bombarding energies. This indeed, has been observed in recent experiments [7–9].

In the γ-vibrational band, the excitation probabilities are enlarged above spin 20 and strongly suppressed below. All these features clearly demonstrate that the rotation-vibration interaction cannot be neglected in collisions of deformed heavy nuclei.

Excitation functions for the 10^+, 20^+ and 26^+ members of the gs- and β-band in ^{238}U are drawn in Figs. 8 and 9, respectively. The upper part of these figures was calculated for pure Coulomb interaction, the lower part contains also nuclear forces. At low projectile energies, P^{Cb} exhibits the typical oscillations of multiple Coulomb excitation. When approaching the Coulomb barrier $E_c \approx 470$ MeV, however, the strong interaction interferes destructively with the Coulomb force, so that the

population of high spin states is considerably reduced. Above the barrier, the nuclear part of the coupling potential dominates (see Fig. 2) and the excitation probabilities rise again.

A similar behaviour can be observed by examining the mean excitation energy $\bar{E}^*$ of the target nucleus as function of bombarding energy (Figure 10). It has been calculated from the asymptotic occupation amplitudes $a_n(t \to +\infty)$ by means of the relation

$$\bar{E}^* = \sum_n |a_n(t \to +\infty)|^2 E_n \,, \tag{5.1}$$

where E_n denote the eigenvalues of the intrinsic Hamiltonian H_0 in Equation (2.1). In the ^{136}Xe-^{238}U collision the maximum excitation energy of the target nucleus amounts to $\bar{E}^*_{^{238}\mathrm{U}} = 2.5$ MeV.

The influence of the rotation-vibration interaction on internal pair formation following nuclear Coulomb excitation will be discussed in a forthcoming paper.

We would like to thank Prof. W. Greiner and Prof. W. Scheid for very fruitful discussions.

Appendix

The functions $F(\mu, r, R_{01}, R_{02})$ together with the limites

$$\lim_{\mu\to 0} \mu^{-2} F(\mu, r, R_{01}, R_{02})$$

and

$$\lim_{\mu\to\infty} F(\mu, r, R_{01}, R_{02})$$

determine the elastic potential $U(r)$. Three different regions for the relative coordinate r have to be investigated: a) both nuclei are well separated, b) the nuclei have a common overlap region, c) the smaller nucleus is completely contained in the larger one. We use the abbreviation

$$x = r - R_{01} - R_{02} \,.$$

The elastic potential function $F(\mu, r, R_{01}, R_{02})$

a) $r > R_{01} + R_{02}$

$$F = \pi \frac{\mu^2}{r} e^{-r/\mu} \left[\left(\frac{\mu}{R_{02}}\right)^2 \sinh\frac{R_{02}}{\mu} - \frac{\mu}{R_{02}} \cosh\frac{R_{02}}{\mu}\right]\left[\left(\frac{\mu}{R_{01}}\right)^2 \sinh\frac{R_{01}}{\mu} - \frac{\mu}{R_{01}} \cosh\frac{R_{01}}{\mu}\right] \tag{A.1}$$

$$\lim_{\mu\to\infty} F = \frac{\pi}{9} R_{01} R_{02}/r \,, \qquad \lim_{\mu\to 0} (\mu^{-2} F) = 0 \,.$$

b) $R_{02} - R_{01} < r < R_{02} + R_{01}$

$$\begin{aligned} F = {} & \pi \frac{\mu^2}{r} e^{-r/\mu} \left[\left(\frac{\mu}{R_{02}}\right)^2 \sinh\frac{R_{02}}{\mu} - \frac{\mu}{R_{02}} \cosh\frac{R_{02}}{\mu}\right]\left[\left(\frac{\mu}{R_{01}}\right)^2 \sinh\frac{R_{01}}{\mu} - \frac{\mu}{R_{01}} \cosh\frac{R_{01}}{\mu}\right] \\ & - \frac{\pi}{2}\left(\frac{\mu^5 \sinh(x/\mu)}{r R_{01} R_{02}^2} + \frac{\mu^5 \sinh(x/\mu)}{r R_{01}^2 R_{02}} + \frac{\mu^4 \cosh(x/\mu)}{r R_{01} R_{02}} + \frac{\mu^6 \cosh(x/\mu)}{r R_{01}^2 R_{02}^2}\right) \\ & + \frac{\pi}{2}\left[\mu^2\left(\frac{x^2}{2r R_{01} R_{02}} + \frac{x^3}{6r R_{01} R_{02}^2} + \frac{x^3}{6r R_{01}^2 R_{02}} + \frac{x^4}{24r R_{01}^2 R_{02}^2}\right)\right. \\ & \left. + \mu^4\left(\frac{1}{r R_{01} R_{02}} + \frac{x}{r R_{01} R_{02}^2} + \frac{x}{r R_{01}^2 R_{02}} + \frac{x^2}{2r R_{01}^2 R_{02}^2}\right) + \frac{\mu^6}{r R_{01}^2 R_{02}^2}\right] \end{aligned} \tag{A.2}$$

$$\lim_{\mu\to\infty} F = \frac{\pi}{9} R_{01} R_{02}/r - \frac{\pi}{2}\left(\frac{x^4}{24r R_{01} R_{02}} + \frac{x^5}{120r R_{01}^2 R_{02}} + \frac{x^5}{120r R_{01} R_{02}^2} + \frac{x^6}{720r R_{01}^2 R_{02}^2}\right),$$

$$\lim_{\mu\to 0} (\mu^{-2} F) = \frac{\pi}{4} \frac{1}{r R_{01} R_{02}}\left(x^2 + \frac{x^3}{3R_{01}} + \frac{x^3}{3R_{02}} + \frac{x^4}{12 R_{01} R_{02}}\right).$$

c) $0 \leqq r < R_{02} - R_{01}$

$$F = \pi \frac{\mu^2}{r} \sinh \frac{r}{\mu} \left[\left(\frac{\mu}{R_{01}} \right)^2 \sinh \frac{R_{01}}{\mu} - \frac{\mu}{R_{01}} \cosh \frac{R_{01}}{\mu} \right] \exp(-R_{02}/\mu) \frac{\mu}{R_{02}} \left(1 + \frac{\mu}{R_{02}} \right) + \frac{\pi}{3} R_{01} \left(\frac{\mu}{R_{02}} \right)^2 ,$$

$$\lim_{\mu \to \infty} F = \pi \left(\frac{R_{01}}{6} - \frac{r^2 R_{01}}{18 R_{02}^2} - \frac{R_{01}^3}{30 R_{02}^2} \right), \qquad \lim_{\mu \to 0} (\mu^{-2} F) = \frac{\pi}{3} \frac{R_{01}}{R_{02}^2} . \tag{A.3}$$

Similarly the functions $G_2(\mu, r, R_{02}, R_{01})$ together with the limites

$$\lim_{\mu \to 0} \mu^{-2} G_2(\mu, r, R_{02}, R_{01}) \quad \text{and} \quad \lim_{\mu \to \infty} G_2(\mu, r, R_{02}, R_{01})$$

determine the radial part of the quadrupole coupling potential for the target nucleus. In the case of projectile excitation one has to interchange the nuclear radii R_{01} and R_{02}.

The quadrupole coupling potential function $G_2(\mu, r, R_{02}, R_{01})$

a) $r > R_{01} + R_{02}$

$$G_2 = 2\pi [f_2(R_{02}) + f_2(-R_{02})] [-f_1(R_{01}) + f_1(-R_{01})] f_2(r) , \tag{A.4}$$

$$\lim_{\mu \to \infty} G_2 = \frac{\pi}{15} \frac{R_{01} R_{02}^2}{r^3}, \qquad \lim_{\mu \to 0} (\mu^{-2} G_2) = 0 .$$

b) $R_{02} - R_{01} < r < R_{02} + R_{01}$

In this section we use the abbreviation $m = m_1 + m_2 + m_3$.

$$\begin{aligned} G_2 = {} & 2\pi [-f_2(R_{02}) f_2(r) f_1(R_{01}) - f_2(-R_{02}) f_2(r) f_1(R_{01}) + f_2(R_{02}) f_2(r) f_1(-R_{01}) - f_2(R_{02}) f_2(-r) f_1(R_{01})] \\ & + 4\pi \sum_{m_1=0}^{2} \sum_{m_2=0}^{2} \sum_{m_3=0}^{1} \sum_{n=0}^{(m+1)/2} \frac{(2+m_1)!}{m_1!\,(2-m_1)!} \frac{(2+m_2)!}{m_2!\,(2-m_2)!} \frac{(1+m_3)!}{m_3!\,(1-m_3)!} \\ & \times \left(\frac{-\mu}{2R_{02}} \right)^{m_1+1} \left(\frac{\mu}{2r} \right)^{m_2+1} \left(\frac{-\mu}{2R_{01}} \right)^{m_3+1} \frac{[(R_{02} + R_{01} - r)/\mu]^{m+1-2n}}{(m+1-2n)!} , \end{aligned} \tag{A.5}$$

$$\begin{aligned} \lim_{\mu \to \infty} G_2 = {} & 2\pi \sum_{m_1=0}^{2} \sum_{m_2=0}^{2} \sum_{m_3=0}^{1} \frac{(2+m_1)!}{m_1!\,(2-m_1)!} \frac{(2+m_2)!}{m_2!\,(2-m_2)!} \frac{(1+m_3)!}{m_3!\,(1-m_3)!} \\ & \times (-2R_{02})^{-m_1-1} (-2r)^{-m_2-1} (-2R_{01})^{-m_3-1} \frac{1}{(m+3)!} \\ & \times [-(R_{02} + r + R_{01})^{m+3} + (-1)^{m_1} (-R_{02} + r + R_{01})^{m+3} \\ & + (-1)^{m_2} (R_{02} - r + R_{01})^{m+3} + (-1)^{m_3+1} (R_{02} + r - R_{01})^{m+3}] , \end{aligned}$$

$$\begin{aligned} \lim_{\mu \to 0} (\mu^{-2} G_2) = {} & 4\pi \sum_{m_1=0}^{2} \sum_{m_2=0}^{2} \sum_{m_3=0}^{1} \frac{(2+m_1)!}{m_1!\,(2-m_1)!} \frac{(2+m_2)!}{m_2!\,(2-m_2)!} \frac{(1+m_3)!}{m_3!\,(1-m_3)!} \\ & \times (-2R_{02})^{-m_1-1} (2r)^{-m_2-1} (-2R_{01})^{-m_3-1} \frac{(R_{02} + R_{01} - r)^{m+1}}{(m+1)!} . \end{aligned}$$

c) $0 \leqq r < R_{02} - R_{01}$

$$G_2 = 2\pi f_2(R_{02}) [f_2(r) + f_2(-r)] [-f_1(R_{01}) + f_1(-R_{01})], \quad \lim_{\mu \to \infty} G_2 = \frac{\pi}{15} \frac{r^2 R_{01}}{R_{02}^3}, \quad \lim_{\mu \to 0} (\mu^{-2} G_2) = 0 . \tag{A.6}$$

The functions $f_1(x)$ and $f_2(x)$ are defined in Equation (3.22).

[1] R. K. Smith, H. Peitz, B. Müller, and W. Greiner, Phys. Rev. Lett. **32**, 554 [1974].
[2] V. Oberacker, G. Soff, and W. Greiner, Phys. Rev. Lett. **36**, 1024 [1976].
[3] V. Oberacker, G. Soff, and W. Greiner, Nucl. Phys. **A259**, 324 [1976].
[4] V. Oberacker, G. Soff, and W. Greiner, Proc. Int. School Seminar On Reactions of Heavy Ions With Nuclei and Synthesis of New Elements, Dubna 1975, p. 235.
[5] W. Betz, G. Heiligenthal, B. Müller, V. Oberacker, J. Reinhardt, W. Schäfer, G. Soff, and W. Greiner, Inv. talk at the Int. Summer School on Nuclear Physics, Predeal, Romania 1976.
[6] B. Müller, V. Oberacker, J. Reinhardt, G. Soff, and W. Greiner, Proc. of the XV Int. Winter Meeting on Nuclear Physics, Bormio (Italy) 1977., p. 243.
[7] P. Colombani, P. A. Butler, I. Y. Lee, D. Cline, R. M. Diamond, F. S. Stephens, and D. Ward, Phys. Lett. **B65**, 39 [1976].
[8] D. Habs, V. Metag, J. Schukraft, H. J. Specht, C. O. Wene, and K. Hildenbrand, Z. Physik A 283, 261 [1977].
[9] G. Franz, H. Ahrens, W. Brüchle, H. Folger, J. V. Kratz, M. Schädel, I. Warnecke, and G. Wirth, GSI Darmstadt, GSI-Bericht J-1-77, p. 41 and G. Franz, private communication.
[10] V. Oberacker, G. Soff, and W. Greiner, "The Dependence of Coulomb Fission on Nuclear Structure", J. Phys. G3, Nr. 12 [1977].
[11] H. Holm and W. Greiner, Nucl. Phys. **A195**, 333 [1972].
[12] F. Videbaek, I. Chernov, P. R. Christensen, and E. E. Gross, Phys. Rev. Lett. **28**, 1072 [1972].
[13] R. A. Broglia, S. Landowne, and A. Winther, Phys. Lett. **40B**, 293 [1972].
[14] I. Y. Lee, J. X. Saladin, C. Baktash, J. E. Holden, and J. O'Brien, Phys. Rev. Lett. **33**, 383 [1974].
[15] H. J. Wollersheim, and Th. W. Elze, Z. Phys. **A280**, 277 [1977].
[16] F. K. McGowan, C. E. Bemis, W. T. Milner, J. L. C. Ford, R. L. Robinson, and P. H. Stelson, Phys. Rev. **C10**, 1146 [1974].
[17] E. Grosse, J. de Boer, R. M. Diamond, F. S. Stephens, and P. Tjøm, Phys. Rev. Lett. **35**, 565 [1975].
[18] E. Grosse, Vielfachcoulombanregung von Rotationszuständen in schweren Kernen, Max-Planck-Institut für Kernphysik, Heidelberg, MPIH-1975-V26.
[19] M. W. Guidry, P. A. Butler, P. Colombani, I. Y. Lee, D. Ward, R. M. Diamond, F. S. Stephens, E. Eichler, N. R. Johnson, and R. Sturm, Nucl. Phys. **A266**, 228 [1976].
[20] N. R. Johnson, R. J. Sturm, E. Eichler, M. W. Guidry, G. D. O'Kelly, R. O. Sayer, D. C. Hensley, N. C. Singhal, and J. H. Hamilton, Phys. Rev. **C12**, 1927 [1975].
[21] P. Fuchs, H. Bokemeyer, H. Emling, E. Grosse, D. Schwalm, H. J. Wollersheim, and D. Pelte, GSI-Bericht J-1-77, Darmstadt; H. J. Wollersheim and E. Grosse, private communication.
[22] A. Winther and J. de Boer, Cal. Inst. of Techn., Report 18-11-65; see also K. Alder, and A. Winther, Coulomb Excitation, Academic Press, New York and London 1966.
[23] V. Oberacker, diploma thesis, Inst. für Theor. Physik, Universität Frankfurt (Main) 1973.
[24] K. Alder and A. Winther, Electromagnetic Excitation — Theory of Coulomb Excitation with Heavy Ions, North-Holland, Amsterdam 1975.
[25] W. Scheid and W. Greiner, Z. Phys. **226**, 364 [1969].
[26] H. J. Fink, W. Scheid, and W. Greiner, Nucl. Phys. **A189**, 259 [1972].
[27] H. A. Bethe, Ann. Rev. Nuc. Sci. **21**, 93 [1971].
[28] V. Oberacker, H. Holm, and W. Scheid, Phys. Rev. **C10**, 1917 [1974].
[29] K. A. Erb, R. R. Betts, D. L. Hanson, M. W. Sachs, R. L. White, P. P. Tung, and D. A. Bromley, Phys. Rev. Lett. **37**, 670 [1976].
[30] A. Faessler, W. Greiner, and R. K. Sheline, Nucl. Phys. **70**, 33 [1965].
[31] J. M. Eisenberg and W. Greiner, Nuclear Theory. Vol. 1, North-Holland, Amsterdam 1970.
[32] B. Müller, V. Oberacker, J. Reinhardt, G. Soff, W. Greiner, J. Rafelski, Invited talk at the Int. Symposium on Nucl. Coll. and their Microscopic Description, Bled (Jugoslavia) 1977.
[33] V. Oberacker, G. Soff, W. Greiner, Proc. of the Int. Conf. on Resonances in Heavy Ion Reactions, Hvar (Jugoslavia) 1977.